Two-dimension tetragonal transition-metal carbides anodes for non-lithium-ion batteries

Changcheng Ke‡, Dong Fan‡, Chengke Chen, Xiao Li, Meiyan Jiang, and Xiaojun Hu*

College of Materials Science and Engineering, Zhejiang University of Technology, Hangzhou 310014, China

‡ These authors contributed equally to this work.

* Corresponding author

E-mail: huxj@zjut.edu.cn (X. Hu)

Table S1 | Calculated structural parameters and atomic positions of *tetr*-MCs with Perdew-Burke-Ernzerhof (PBE) functional.

tetr-MCs	Functional	Lattice parameters (Å)			Metal atomic positions			Carbon atomic positions		
		a	***b***	***c***	*x*	*y*	*z*	*x*	*y*	*z*
ScC		3.22	3.22	2.30						
TiC		2.99	2.99	2.15						
VC		2.86	2.86	2.04	0.00	0.00	0.38	0.50	0.50	0.38
CrC	PBE	2.79	2.79	1.97						
ZrC		3.27	3.27	2.24	0.50	0.50	0.44	0.00	0.00	0.45
NbC		3.10	3.10	2.17						
TaC		3.09	3.09	2.19						
HfC		3.23	3.23	2.23						

Table S2 | Calculated elastic constants, in-plane Young's modulus and Poisson's ratio of *tetr*-MCs at GGA-PBE level.

Phase	C_{11}/GPa	C_{22}/GPa	C_{12}/GPa	C_{66}/GPa	In-plane stiffness /GPa·nm	Poisson's ratio
tetr-CrC	263.8	263.8	121.5	134.8	207.8	0.46
tetr-HfC	248.6	248.6	73.7	114.7	226.8	0.30
tetr-NbC	288.9	288.9	92.5	126.8	259.3	0.32
tetr-ScC	167.5	167.5	71.3	22.8	137.2	0.43
tetr-TaC	327.2	327.2	114.4	151.2	287.2	0.35
tetr-TiC	239.1	239.1	80.0	124.6	212.3	0.33
tetr-VC	255.1	255.1	101.0	133.8	215.1	0.40
tetr-ZrC	231.1	231.1	63.8	100.0	213.5	0.28

Table S3 | Calculated the volume expansion, in-plane stiffness and Poisson's ratio of *tetr*-VC with increased concentrations of Mg ions.

tetr-VCMg$_x$	In-plane stiffness /GPa·nm	Poisson's ratio	Change in lattice parameters(Å)					
			Before optimization			End of optimization		
			a	***b***	***c***	***a***	***b***	***c***
x=1	254.8	0.35	2.864	2.864	2.184	2.899	2.899	2.008
x=1.5	301.8	0.25	2.864	2.864	2.022	2.911	2.911	2.008
x=2	350.8	0.15	2.864	2.864	2.022	2.924	2.924	1.995

Table S4 | The adsorption energies of Mg atom on C site, hole site, and V site, respectively.

Phase	Adsorption energy (eV)		
Adsorption position	C site	Hole site	V site
tetr-CrC	-1.45	-1.52	-1.21
tetr-HfC	-0.77	-0.63	-0.70
tetr-NbC	-0.52	-0.19	-0.19
tetr-ScC	-1.76	-2.13	-1.75
tetr-TaC	-1.41	-1.09	-1.01
tetr-TiC	-0.67	-0.64	-0.65
tetr-VC	-1.12	-1.07	-0.89
tetr-ZrC	-0.78	-0.62	-0.67

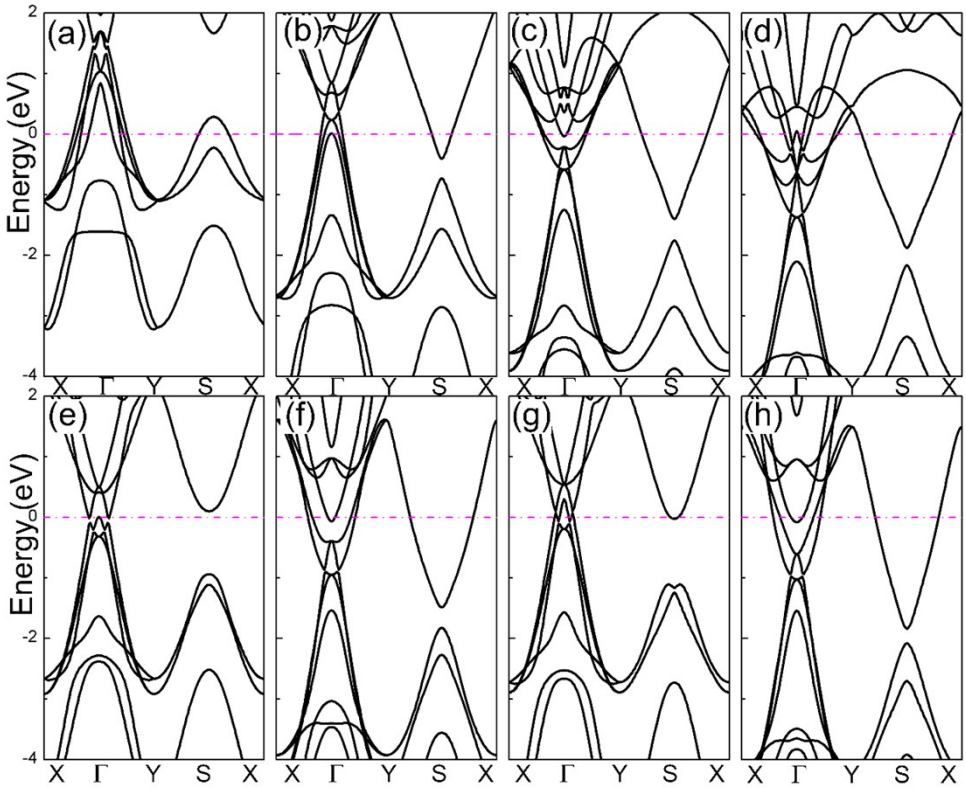

Fig. S1 | Electronic band structure of (a-h) *tetr*-ScC, *tetr*-TiC, *tetr*-VC, *tetr*-CrC, *tetr*-ZrC, *tetr*-NbC, *tetr*-TaC, and *tetr*-HfC with PBE functional, respectively. The Fermi level is set as 0 eV. Γ (0, 0, 0), X (1/2, 0, 0), S (1/2, 1/2, 0) and Y (0, 1/2, 0) refer to special points in the first Brillouin zone of reciprocal space.

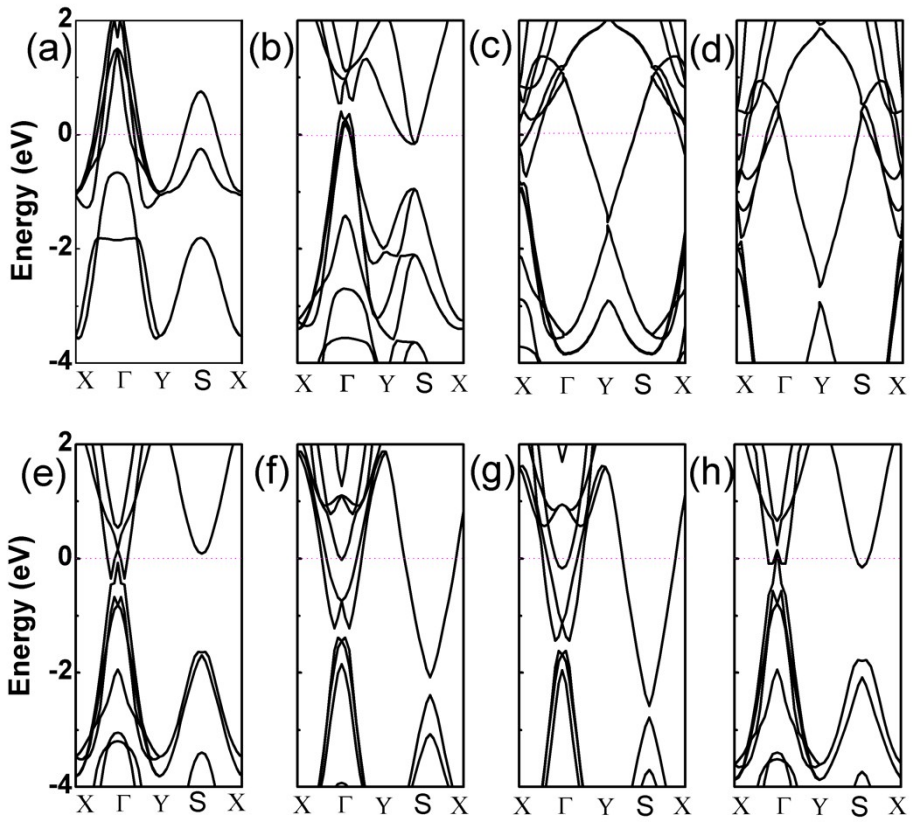

Fig. S2 | Electronic band structure of (a-h) *tetr*-ScC, *tetr*-TiC, *tetr*-VC, *tetr*-CrC, *tetr*-ZrC, *tetr*-NbC, *tetr*-TaC, and *tetr*-HfC with Heyd-Scuseria-Ernzerhof (HSE06) functional, respectively. The Fermi level is set as 0 eV. Γ (0, 0, 0), X (1/2, 0, 0), S (1/2, 1/2, 0) and Y (0, 1/2, 0) refer to special points in the first Brillouin zone of reciprocal space.

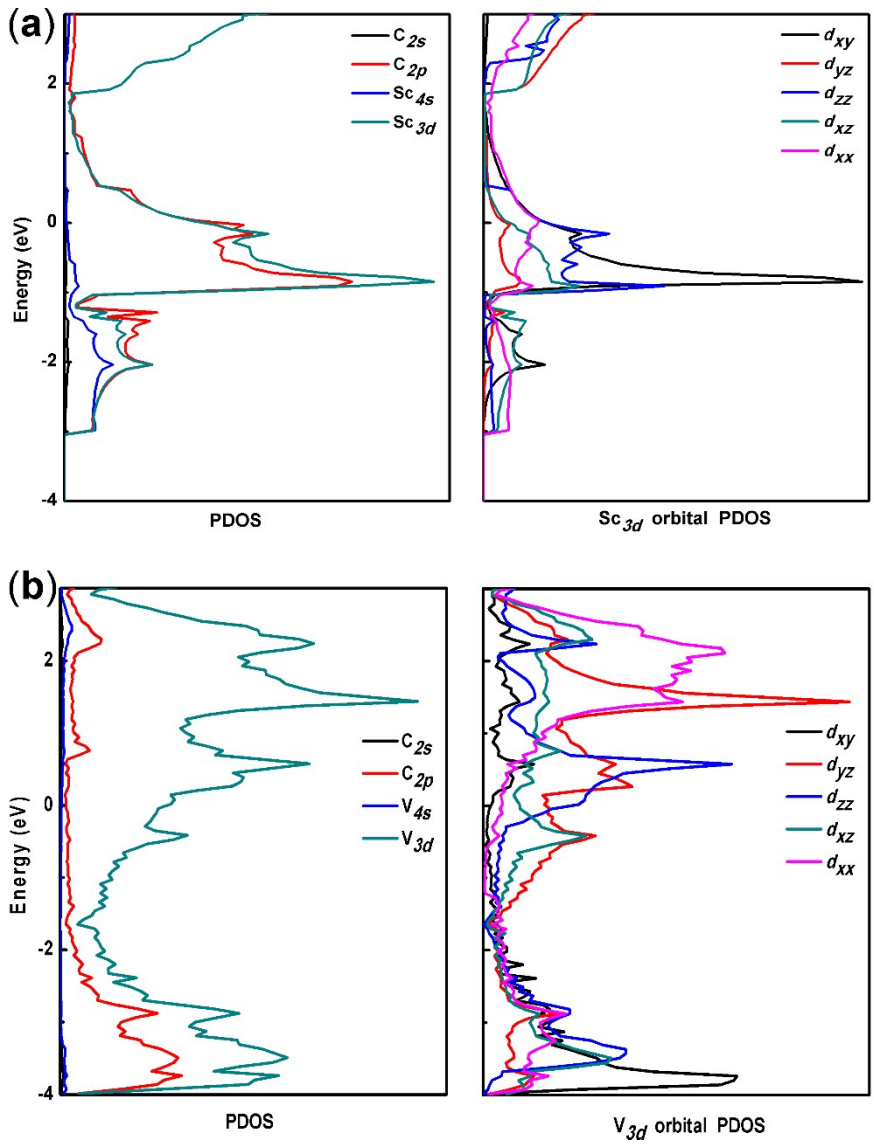

Fig. S3 | Partial density of states (DOS) of (a) *tetr*-ScC and (b) *tetr*-VC at equilibrium state.

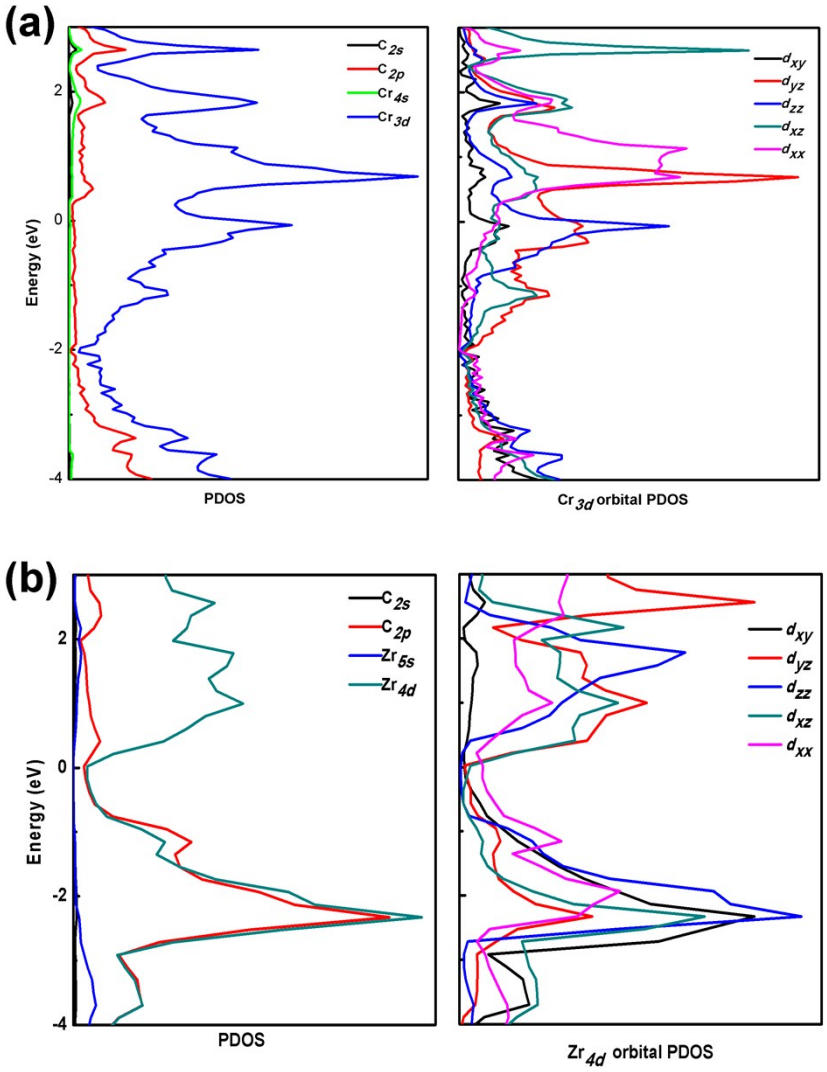

Fig. S4 | Partial DOS of (a) *tetr*-CrC and (b) *tetr*-ZrC at equilibrium state.

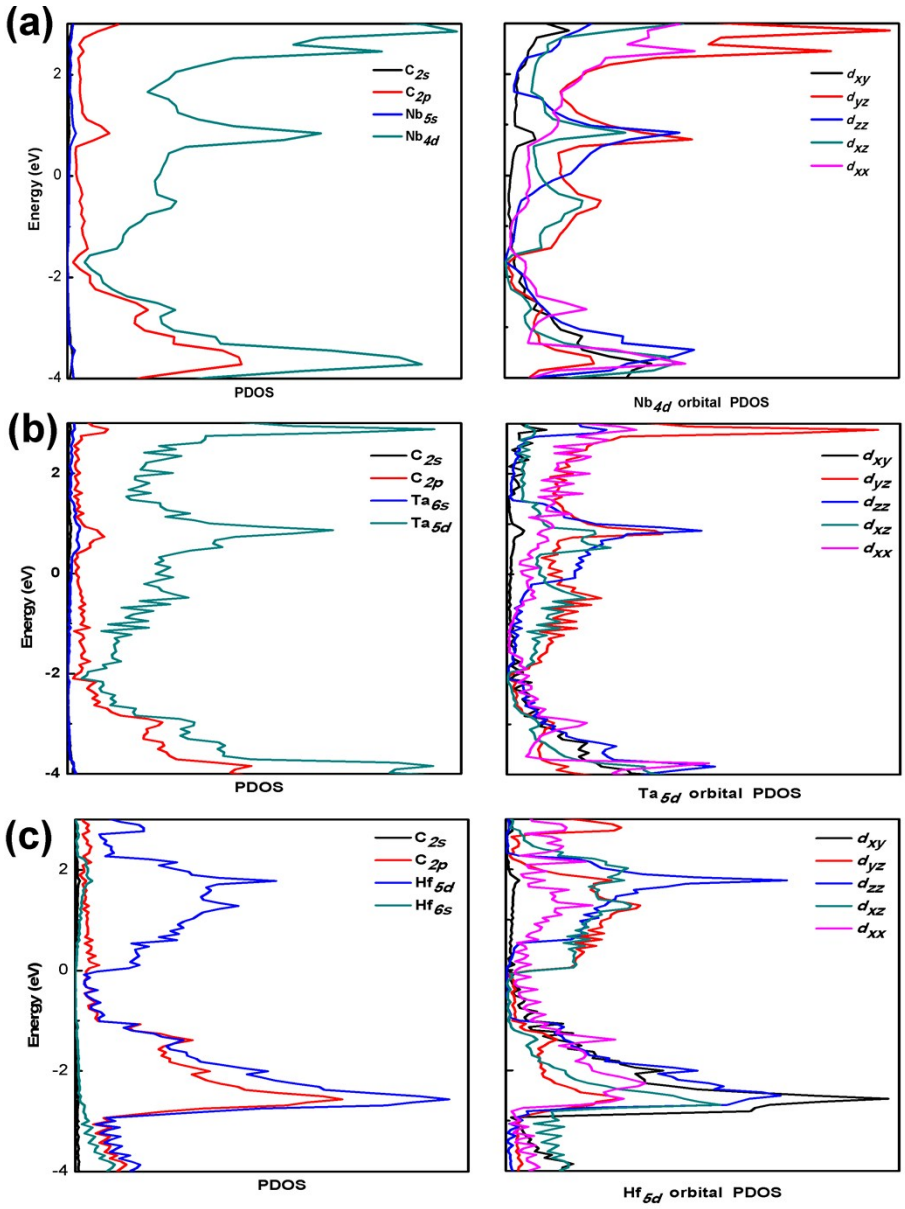

Fig. S5 | Partial DOS of (a) *tetr*-NbC, (b) *tetr*-TaC and (c) *tetr*-HfC at equilibrium state.

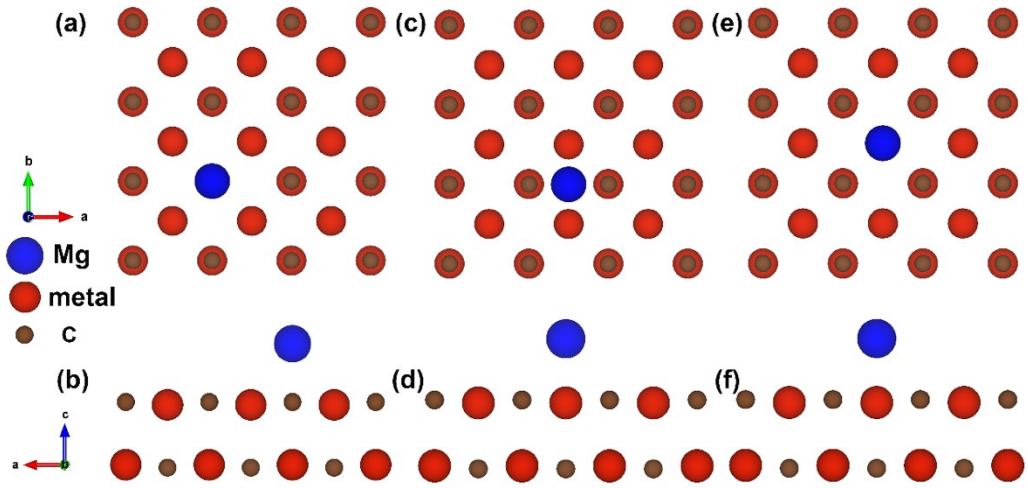

Fig. S6 | The top views of Mg atom located directly on (a) C site, (c) hole site and (e) metal site on *tetr*-MCs, respectively. And the side views of Mg atom located directly on (b) C site, (d) hole site, (f) metal site on *tetr*-MCs, respectively. The blue, red and brown spheres represent Mg, metal, and C atoms, respectively.

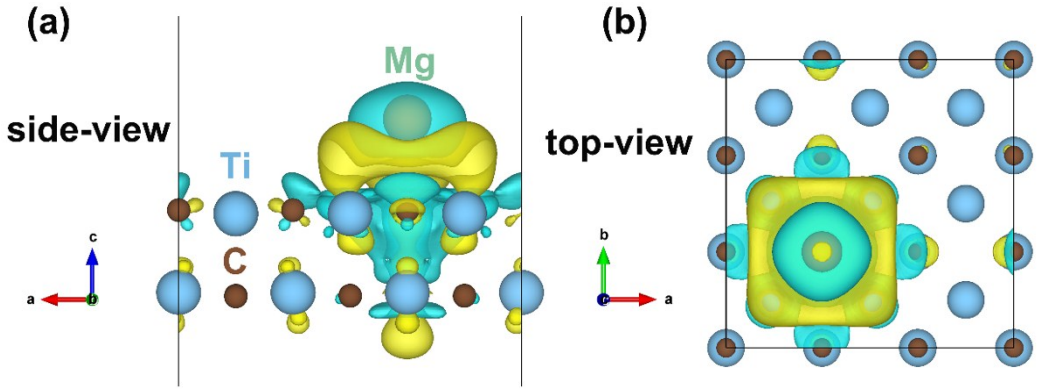

Fig. S7 | The (a) side-view and (b) top-view of charge density differences for the Mg atom on *tetr*-TiC surface. The yellow and light blue regions represent the electron accumulation and depletion, respectively.

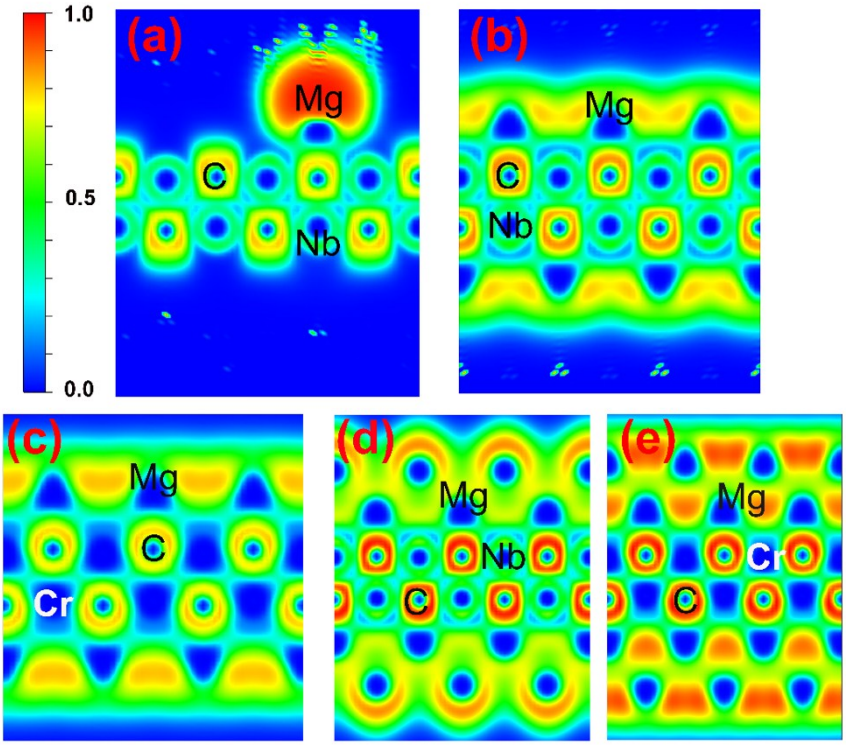

Fig. S8 | The electron localization function (ELF) maps of (a) single Mg atom on *tetr*-NbC, (b) one layer of Mg atoms on *tetr*-NbC, (c) one layer of Mg atoms on *tetr*-CrC, (d) two layers of Mg atoms on *tetr*-NbC, and (e) two layers of Mg atoms on *tetr*-CrC. ELF ranges from 0.0 (blue) to 1.0 (red).

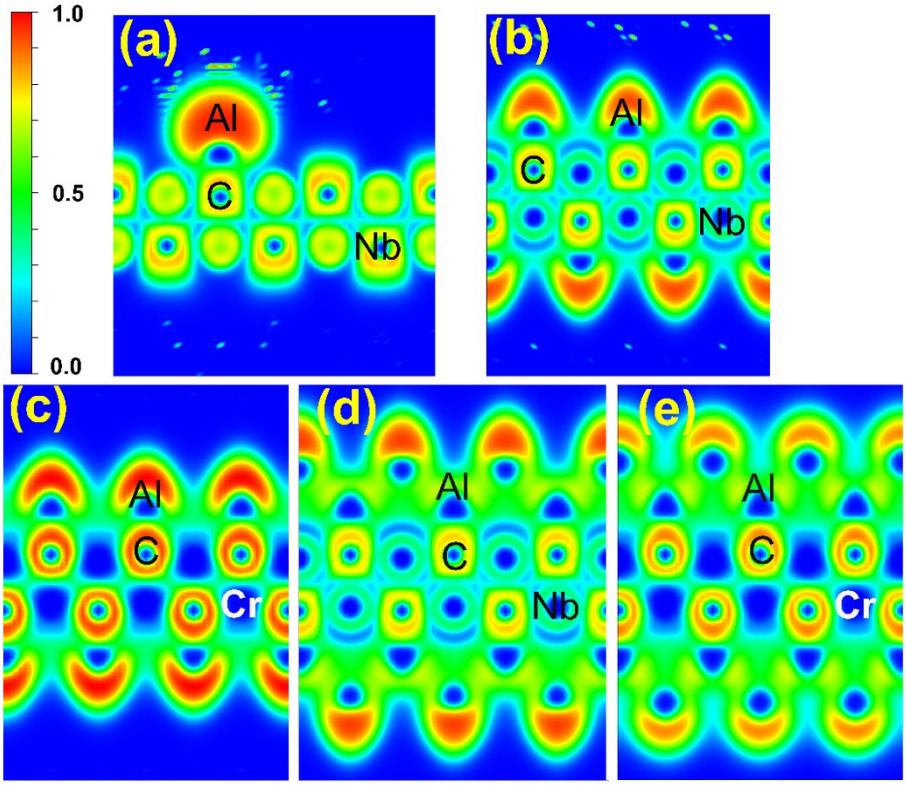

Fig. S9 | The ELF maps of (a) single Al atom on *tetr*-NbC, (b) one layer of Al atoms on *tetr*-NbC, (c) one layer of Al atoms on *tetr*-CrC, (d) two layers of Al atoms on *tetr*-NbC, and (e) two layers of Al atoms on *tetr*-CrC. ELF ranges from 0.0 (blue) to 1.0 (red).

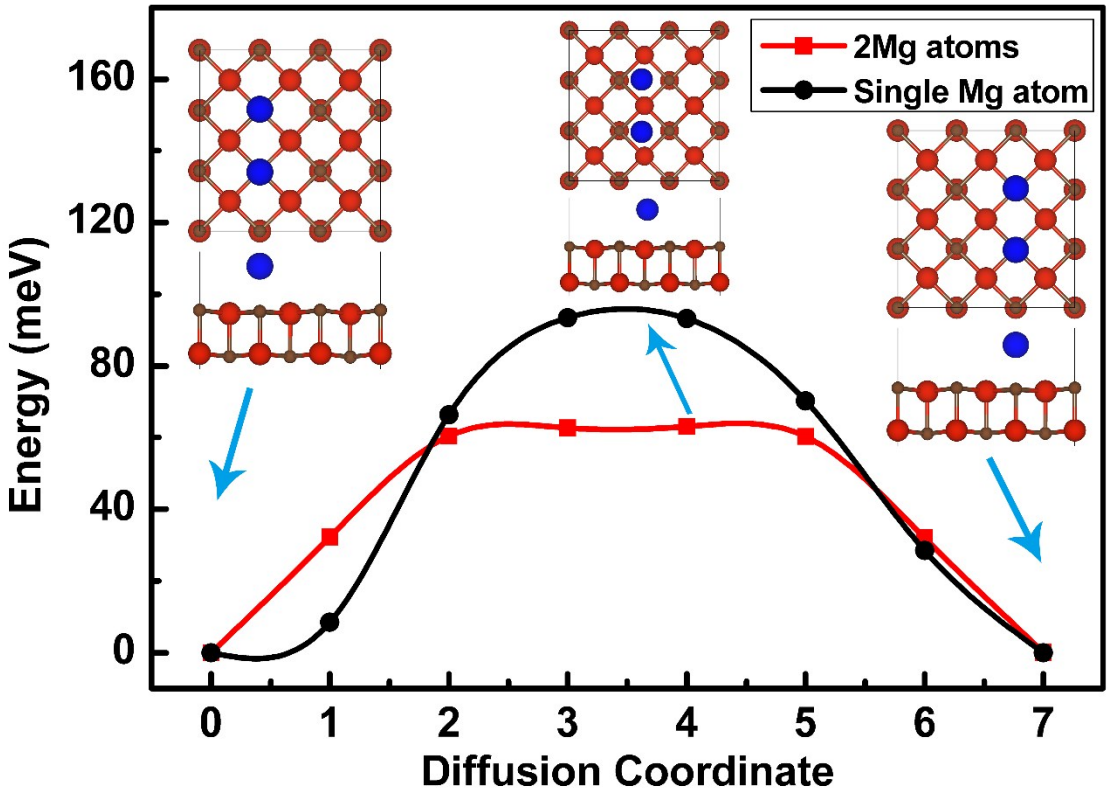

Fig. S10 | The diffusion energy barrier of single Mg atom and two Mg atoms on *tetr*-VC. The internal illustrations correspond to the initial, transition state, and final structures, respectively. The blue balls, red balls, and brown balls represent Mg atoms, V atoms, and C atoms, respectively.